Solid Freeform Fabrication 2018: Proceedings of the 29th Annual International Solid Freeform Fabrication Symposium – An Additive Manufacturing Conference
Reviewed Paper

Investigation into the crystalline structure and *sub-T_{pm}* exotherm of selective laser sintered Polyamide 6

Peng Chen, Shifeng Wen, Chunze Yan *, Jie Liu*, Yusheng Shi

State key Laboratory of Materials Processing and Die & Mould Technology, School of Materials Science and Engineering, Huazhong University of Science and Technology, Wuhan 430074, China.

Abstract

Selective Laser Sintering (SLS) has achieved a wide acceptance for direct manufacture of complex functional components. However, the performance of SLS part still needs to be improved, in which the crystalline structure plays an important role. Every crystalline form has specific properties, and the whole material behaviors have great relationships with the various species and crystalline structure. Therefore, this paper investigates crystalline structure of laser sintered Polyamide 6 (PA6) and quantifies the different HT-α and LT-α phases using thermal analysis. The results show that the sintered parts are uniformly characterized by a relatively stronger (2 0 0) and a weaker (0 0 2) diffraction peak. This crystalline structure variation is basically consistent for all SLS parts and independent of laser power. In addition, the *sub-T_{pm}* crystallization transition concerning α phase was found for SLS PA6 part, which is derived from the release of strain energy absorbed during SLS processing.

Key words: Additive Manufacturing (AM), Selective Laser Sintering (SLS), Polyamide 6 (PA6), Crystalline Structure

*Corresponding author. Tel: +86(0)2787558155. E-mail address: c_yan@hust.edu.cn (C. Yan), hustliuj@mail.hust.edu.cn (J. Liu).

1.Introduction

Polyamides (PA) have much better thermo-mechanical properties than polyolefins which make them more suitable for applications requiring creep and fatigue resistance in the automotive industry. Using of high-performance PA6 (also known as polycaprolactam and nylon 6) materials in place of conventional metal materials has been growing in the manufacturing of structural parts, such as manufacturing of parts in the engine compartments, bearings and gears [1-5]. Currently, there appears a demand of integrated manufacturing that combines complex structures and good mechanical properties, such as automobile cylinder head. In this case, the traditional tooling method will be no longer fit and Additive Manufacturing (AM) will be a smarter choice.

Selective Laser Sintering (SLS), one of the most promising polymeric AM technologies, can fabricate complex 3D structures via selectively fusing successive layers of powdered material. The principal advantage of SLS is the ability to manufacture parts with great complexity of geometry accompanied with good tensile strength and elastic modulus comparable to their injection moulded counterparts [6]. However, the laser sintered parts with good mechanical properties are mainly limited to long-chain polyamides, such as PA12 and PA11 [6, 7]. The performance of SLS PA6 part still needs to be improved, in which the crystalline structure plays an important role [8-10].

PA6 has two common crystalline forms: the α and γ forms [11]. It is generally believed that the α form (monoclinic crystal) is more thermodynamically stable and has a higher Young's modulus compared to the γ form (hexagonal/pseudohexagonal crystal) [12]. These two crystalline forms usually coexist in materials with different compositions depending largely on processing conditions. As for SLS, the laser sintered PA6 material exhibited a combination of two different α crystal forms (HT-α and LT-α forms) [13]. Both crystal forms are matched to distinct regions within the material's observable microstructure. The presence of unmolten particle cores (LT-α) makes the laser sintered material a composite-like structure and may have important influence on

mechanical properties. Therefore, the aim of this paper is to investigate the crystalline structure and composition of laser sintered PA6 and make the connection with mechanical properties.

2.Experiment

2.1 Material and SLS process

The material used for investigation is virgin PA6 powder obtained from Solvay S.A. Group. Laser sintering process of the powder was carried out on a self-developed machine HK-P320 with a CO_2 laser (wavelength 10.6 μm, laser beam diameter 0.4 mm) [14]. In order to investigate the influence of laser power on crystalline structure and composition, different levels of laser power were selected, while other parameters, i.e. laser scan spacing (s), layer thickness (h) and powder bed temperature (T_b) were set as constant values. All the processing parameters are listed as shown in Table. 1.

Table. 1 SLS processing parameters for PA6 powder

Materials	Bed temp. (℃)	Laser power (W)	Scan velocity (mm/s)	Scan spacing (mm)	Layer thickness (mm)
PA6	195	20, 25, 30	4000	0.3	0.12

2.2 Characterization

Thermal analysis experiments of powder and laser sintered samples were conducted on a Diamond DSC (PerkinElmer Instruments, USA) under nitrogen protecting atmosphere and the heating rate was set as 10 °C/min. The determination of special points such as onset and end point of melting, and the calculation of melting enthalpy were performed using TA Universal Analysis 2000 software. The degree of crystallinity X_C can be calculated using the formula below:

$$X_C = \frac{\Delta H_m}{\Delta H_m^0} \times 100\% \quad (1)$$

where the ΔH_m is the melt enthalpy of sample and the ΔH_m^0 is the melt enthalpy of the perfect crystal. The melt enthalpy for 100% crystalline PA6 material was taken as 230 J/g [11]. The polymorphism and crystalline characteristics were analyzed on a X'Pert3 powder X-ray diffractometer (PANalytical B.V., Netherlands) with a PIXcel

detector, using Cu Kα radiation at scan speed 3°/min. X'pert-HighScore Plus 3.0.5 software was utilized for experimental data handling and analysis. Tensile samples were prepared according to the standard ASTM D638-03 Type Ⅴ. The tensile tests were performed on E1000 (Instron-Division of ITW Limited) instrument at the tensile speed of 1 mm/min. Four samples were used for the calculation of average data.

3.Results and discussion

3.1 Thermal Analysis and Quantification of HT-α and LT-α Phases

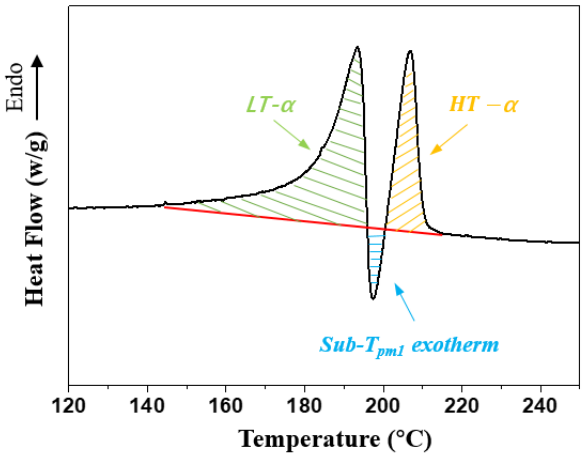

Figure. 1 Schematic diagram of HT-α and LT-α crystalline forms. DSC heating curve of sample laser sintered at 20W, 4000 mm/s.

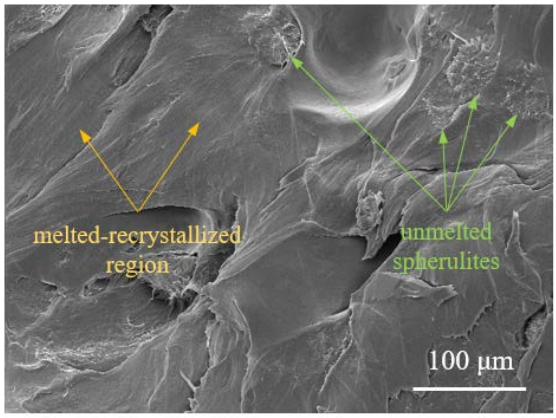

Figure. 2 Distinct microstructure of tensile failure section corresponding to different crystal forms.

Just as Figure. 1 shows, the laser sintered PA6 sample usually has two different α crystalline forms (HT-α and LT-α), which correspond to the high-temperature melting

peak T_{pm1} and the low-temperature melting peak T_{pm2}. The LT-α form is related to the melted-recrystallized region, while the HT-α is the unmelted particle spherulites that is essentially the laser-affected powder material [13]. What is unfamiliar is that the laser sintered PA6 has a *sub*-T_{pm1} crystallization exotherm concerning α phase. This *sub*-T_{pm1} exothermic peak locates at DSC heating curve between HT-α and LT-α endotherms, which is derived from the release of strain energy absorbed during SLS processing and cannot be found in PA12 [13, 15, 16].

Both crystal forms are matched to distinct regions within the material's observable microstructure as shown in Figure. 2. This makes the laser sintered PA6 behave as a micro-composite material. Therefore, the content of unmelted particle spherulites (reinforcement phase) and their interface connected with melted-recrystallized region become the main factors influencing mechanical properties. In order to figure out their influence on mechanical properties, we quantificationally calculate the enthalpies of HT-α, LT-α and *sub*-T_{pm1} exotherm of samples sintered at different laser power using DSC. The DSC curves of all samples are shown in Figure. 3 and the calculation results are shown in Table. 2. It can be seen that with the increase of laser power, the relative content of ΔH_m^{LT} is increasing and the value of ΔH_m^{HT} is becoming smaller. This suggests that the relative quantity of unmelted particle spherulites is reducing, and thus the interface with melted-recrystallized region becomes less. Their effect on mechanical properties will be discussed in the section 3.3.

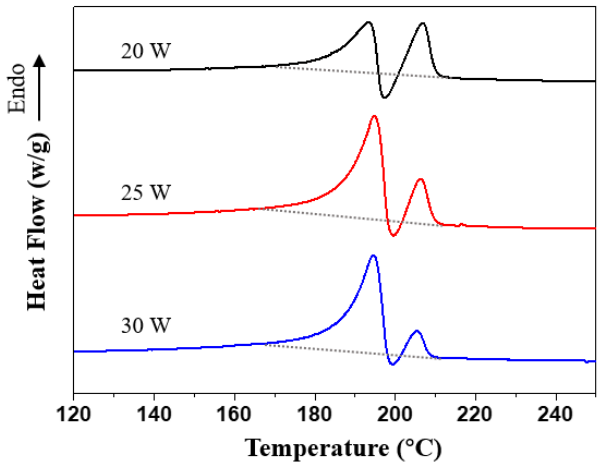

Figure. 3 DSC curves of sintered PA6 at different laser power.

Table. 2 Quantitative data of thermal properties of HT-α and LT-α phases

Laser power	Melting enthalpy (J/g)		Crystallinity (%)			*Sub-T_{pm1}* exotherm (J/g)
	ΔH_m^{LT}	ΔH_m^{HT}	X_c^{LT}	X_c^{HT}	X_c^{α}	
20W	29.88 (59.81%)	20.08 (40.19%)	12.99	8.73	21.72	5.75
25W	39.66 (80.97%)	9.39 (19.03%)	17.24	4.08	21.32	1.69
30W	37.05 (88.09%)	5.01 (11.91%)	16.11	2.18	18.29	1.72

** The relative content of HT-α (LT-α) in α is inside the parentheses.*

3.2 Analysis of Crystalline Structure

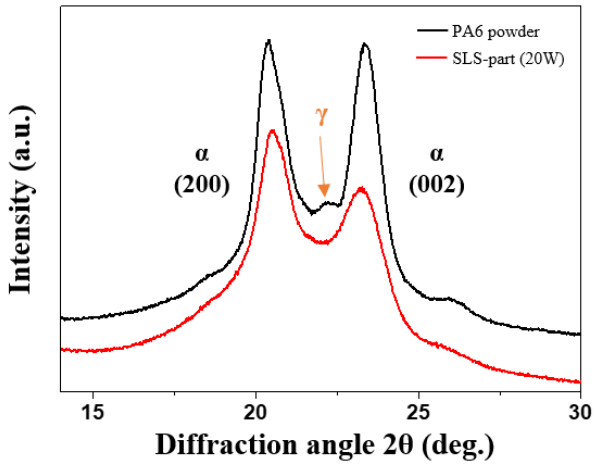

Figure. 4 Crystalline structure of PA6 powder and laser sintered sample at 20W.

Figure. 4 illuminates the crystalline structure difference caused by SLS. It can be seen that the XRD curve of powder is mainly featured by two α peaks corresponding to the diffraction of (2 0 0) and (0 0 2) planes respectively. The (2 0 0) plane contains chains only linked by van der Waals forces, whereas the (0 0 2) refers to the hydrogen-bonded sheets [11]. Both two diffraction peaks have similar intensities. However, after SLS processing, these two peaks are depressed more or less. From the XRD curve of laser sintered part, it is easy to find out that the hydrogen-bonded (0 0 2) plane is more influenced and weaker than (2 0 0). This suggests that the diffraction intensity of

hydrogen-bonded planes (0 0 2) is more sensitive to laser than that of (2 0 0) revealing the more pronounced influence of laser on the H-bonds as compared to van der Waals interactions. In order to make it clear that if there are the same phenomena for all sintered samples, the XRD data of samples sintered at different laser power were collected (Figure. 5).

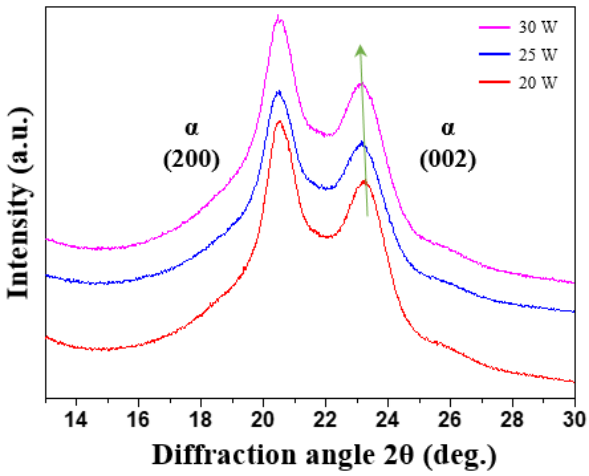

Figure. 5 Crystalline structure of laser sintered sample at 20W, 25W, 30W respectively.

Unexpectedly, all the XRD curves exhibit similar peaks with a stronger (2 0 0) and a weaker (0 0 2). This further proves that the diffraction intensity of hydrogen-bonded planes (0 0 2) is more sensitive to laser than that of (2 0 0). In addition, what should be noted is that diffraction angle of (0 0 2) is decreasing with the increase of laser power. According to the Bragg equation, it can be concluded that the interplanar spacing of (0 0 2) is increasing. This may be attributed to the chain growth of melt-state polycondensation which happens during the laser sintering process [14]. What's more, after SLS processing, the inconspicuous γ peak of the powder experiences the melt-recrystallization process and can be hardly found in the laser sintered part. This means that the crystallization of laser sintered melt is similar to that of normal melt-crystallization and tends to form α phase.

3.3 Mechanical Properties and Connection with Phase Composition and Crystallinity

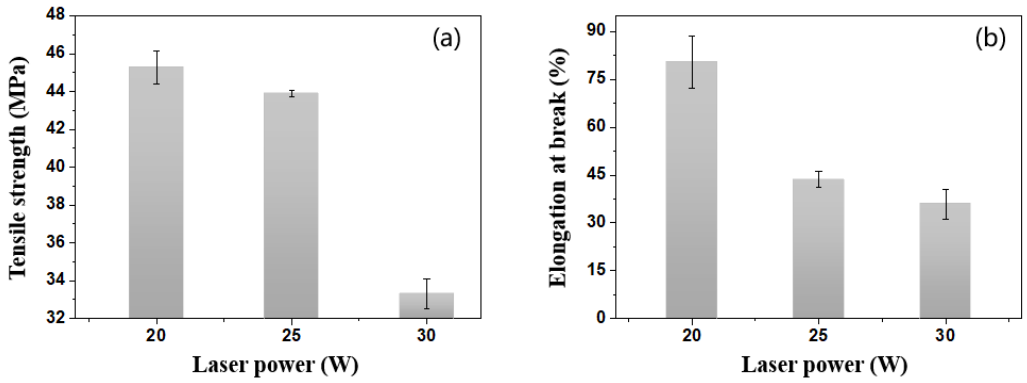

Figure. 6 Tensile strength (a) and elongation at break (b) of laser sintered sample at 20W, 25W, 30W respectively.

Figure. 6 shows the results of tensile tests, and the data are shown in Table. 3. It can be seen that the 20W sintered part has the highest tensile strength (TS) and elongation at break (EB). Interestingly, it is worth to note that the 20W sintered part also has the maximum value of ΔH_m^{HT} and *Sub-*T_{pm1} crystallization enthalpy, suggesting a high content of unmelted particle spherulites (reinforcement phase) and abundant interface connected with melted-recrystallized region. What more, the crystallinity of α phase (X_c^{α}) of 20W sintered part is also the largest. This means that there may be some connection between mechanical properties and phase composition. In order to figure out the relationships between the phase composition, crystallinity of α phase and mechanical properties, the Figure. 7 is plotted.

Table. 3 Data of PA6 tensile tests at different laser power.

Mechanical properties	**PA6 sintered at different laser power**		
	20W	**25W**	**30W**
TS (MPa)	45.84±0.88	44.45±0.19	33.88±0.78
EB (%)	81.02±8.11	44.16±2.55	36.54±4.67

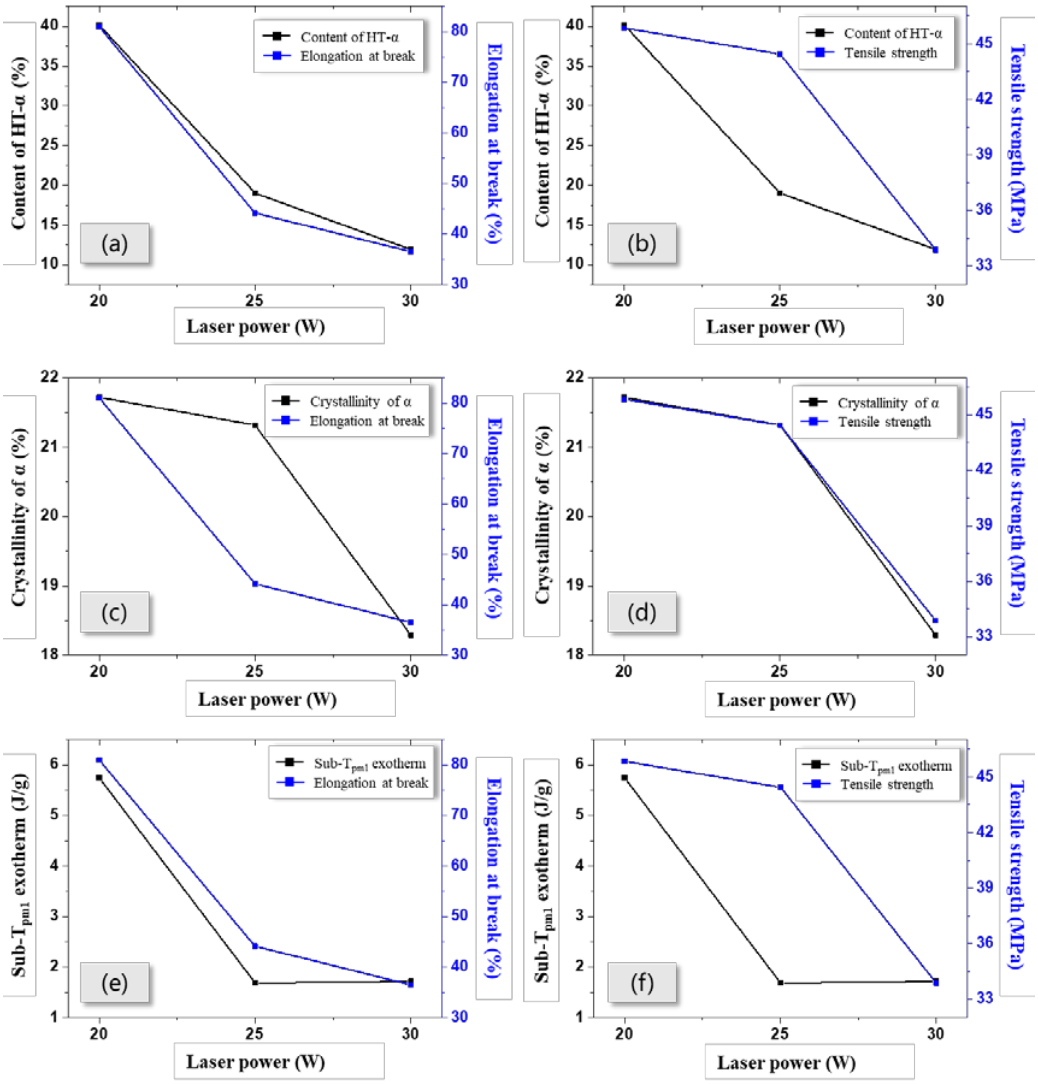

Figure. 7 The relationships between (a) relative content of HT-α and elongation at break, (b) relative content of HT-α and tensile strength, (c) crystallinity of α phase and elongation at break, (d) crystallinity of α phase and tensile strength.

It can be seen from Figure.7 that in general, the relative content of HT-α, the crystallinity of α phase and the Sub-T_{pm1} exotherm have the similar decreasing trend as tensile strength and elongation at break in the 20~30W. This suggests that in this laser power range, the higher content of HT-α, crystallinity of α phase and Sub-T_{pm1} exotherm are more beneficial to the tensile strength and elongation at break. Furthermore, it is easy to find that the Figure.7a, 7d, 7e have the basically identical trends, which are different from those of Figure.7b, 7c, 7f. Therefore, we can further

conclude that in comparison with the crystallinity, the elongation at break has stronger correlation with content of HT-α (unmelted particle spherulites) and Sub-T_{pm1} exotherm (interface connected with melted-recrystallized region). On the contrary, the tensile strength has a stronger correlation with crystallinity rather than the content of HT-α and Sub-T_{pm1} exotherm.

In section 3.2 (Figure.4), we can easily identify that the powder has a more perfect crystalline structure and higher crystallinity of α than the sintered part due to its sharper α peaks and greater integral area. The more perfect crystalline structure usually has a better mechanical property. As is concluded above, the higher crystallinity of α phase is more beneficial to the tensile strength, and the higher content of HT-αand Sub-T_{pm1} exotherm is more beneficial to the elongation at break. Therefore, we can conclude that sintered parts obtained by complete melting of powder do not definitely have the best the tensile properties due to the lower crystallinity and less reinforcement phase. In fact, an appropriate amount of unmelted powder would be more beneficial to mechanical properties.

4.Conclusion

Mechanical properties have great relationships with the crystalline structure and composition. In this paper, we investigate the crystalline structure of laser sintered PA6 using XRD, and quantitatively analyze the phase composition through DSC. The relationships between mechanical properties and phase composition and crystallinity are also discussed. The main conclusions are:

- The XRD curves of laser sintered parts exhibit similar peaks with a stronger (2 0 0) and a weaker (0 0 2) because the diffraction intensity of hydrogen-bonded (0 0 2) plane is more sensitive to laser than that of (2 0 0).
- In comparison with the crystallinity, the elongation at break has stronger correlation with content of HT-α and Sub-T_{pm1} exotherm. On the contrary, the tensile strength has a stronger correlation with crystallinity rather than the content of HT-α and Sub-T_{pm1} exotherm.
    - The sintered PA6 parts obtained by complete melting of powder do not

definitely have the best the tensile properties due to the lower crystallinity and less reinforcement phase. An appropriate amount of unmelted powder would be more beneficial to mechanical properties.

Reference

[1] C.M. Sonsino, E. Moosbrugger, Fatigue design of highly loaded short-glass-fibre reinforced polyamide parts in engine compartments, International Journal of Fatigue 30(7) (2008) 1279-1288.

[2] A. Benaarbia, A. Chrysochoos, G. Robert, Thermomechanical behavior of PA6.6 composites subjected to low cycle fatigue, Composites Part B-engineering 76 (2015) 52-64.

[3] L. Chang, Z. Zhang, H. Zhang, A.K. Schlarb, On the sliding wear of nanoparticle filled polyamide 66 composites, Composites Science and Technology 66(16) (2006) 3188-3198.

[4] A. Bernasconi, P. Davoli, A. Basile, A. Filippi, Effect of fibre orientation on the fatigue behaviour of a short glass fibre reinforced polyamide-6, International Journal of Fatigue 29(2) (2007) 199-208.

[5] S. Mortazavian, A. Fatemi, Fatigue behavior and modeling of short fiber reinforced polymer composites: A literature review, International Journal of Fatigue 70(Supplement C) (2015) 297-321.

[6] R.D. Goodridge, C.J. Tuck, R.J.M. Hague, Laser sintering of polyamides and other polymers, Progress in Materials Science 57(2) (2012) 229-267.

[7] S. Berretta, K.E. Evans, O. Ghita, Processability of PEEK, a new polymer for High Temperature Laser Sintering (HT-LS), European Polymer Journal 68(Supplement C) (2015) 243-266.

[8] S. Das, S.J. Hollister, C.L. Flanagan, A. Adewunmi, K. Bark, C. Chen, K. Ramaswamy, D. Rose, E. Widjaja, Freeform fabrication of Nylon-6 tissue engineering scaffolds, Rapid Prototyping Journal 9(1) (2003) 43-49.

[9] G.V. Salmoria, J.L. Leite, L.F. Vieira, A.T.N. Pires, C.R.M. Roesler, Mechanical properties of PA6/PA12 blend specimens prepared by selective laser sintering, Polymer Testing 31(3) (2012) 411-416.

[10] S. Rhee, J.L. White, Crystal structure, morphology, orientation, and mechanical properties of biaxially oriented polyamide 6 films, Polymer 43(22) (2002) 5903-5914.

[11] J. Pepin, V. Miri, J.-M. Lefebvre, New Insights into the Brill Transition in Polyamide 11 and Polyamide 6, Macromolecules 49(2) (2016) 564-573.

[12] L.S. Loo, K.K. Gleason, Insights into Structure and Mechanical Behavior of α and γ Crystal Forms of Nylon-6 at Low Strain by Infrared Studies, Macromolecules 36(16) (2003) 6114-6126.

[13] P. Chen, H. Wu, W. Zhu, L. Yang, Z. Li, C. Yan, S. Wen, Y. Shi, Investigation into the processability, recyclability and crystalline structure of selective laser sintered Polyamide 6 in comparison with Polyamide 12, Polymer Testing.

[14] P. Chen, M. Tang, W. Zhu, L. Yang, S. Wen, C. Yan, Z. Ji, H. Nan, Y. Shi, Systematical mechanism of Polyamide-12 aging and its micro-structural evolution during laser sintering, Polymer Testing 67 (2018) 370-379.

[15] S. Dadbakhsh, L. Verbelen, O. Verkinderen, D. Strobbe, P. Van Puyvelde, J.-P. Kruth, Effect of PA12 powder reuse on coalescence behaviour and microstructure of SLS parts, European Polymer Journal (2017).

[16] N. Hopkinson, C.E. Majewski, H. Zarringhalam, Quantifying the degree of particle melt in

Selective Laser Sintering®, CIRP Annals - Manufacturing Technology 58(1) (2009) 197-200.